Supplemental Materials.

(Supplemental Text, Figures, and Table).

Supplemental Text.

Computational model for melanosome aggregation.

To model melanosome aggregation kinetics we used a discrete spatial 2D stochastic model in which each object (MT or melanosome) is treated as a discrete entity (Lomakin et al., 2009). The results of this stochastic modeling were further supported by a separate set of equations that were used to calculate melanosome densities. These equations are referred to as our continuous approach or course-grained analysis, and they fully supported the results of the stochastic model.

Stochastic model for melanosome aggregation.

The stochastic model allowed us to compute how fast the peripheral cytoplasm becomes free of pigment granules, which we refer to as grey level kinetics. This computation is based on experimentally determined values for MT and melanosome number, the parameters of MT dynamics, the probability of pigment granule capture by growing MT tips decorated with CLIP-170, and parameters of bidirectional movement of captured melanosomes to the cell center. In the model, we used the following assumptions:

(1). The cell was approximated with a disc with a radius of 27 μm based on the average radius and negligible height of a *Xenopus* melanophore.
(2). MTs were modeled as radial lines with their minus ends clustered in the cell center and the plus ends extended to the periphery (Suppl. Fig. 1A).
(3). MTs were uniformly distributed around the cell center (had uniform angular distribution).
(4). Growing MTs immediately began shortening when they reached the cell boundary.
(5). Shortening MTs immediately began growing when they reached the cell center.
(6). All MTs bound pigment granules with equal probability.
(7). Binding of pigment granules to MTs occurred only at growing tips, all of which were decorated with CLIP-170.
(8). Transition rates between different MT states of polymerization and melanosome states of movement were determined using steady state approximation. We assumed that the fractions of growing, shortening and pausing MTs, and the fractions of melanosomes moving to MT plus or minus ends or pausing equal to their corresponding average values measured at steady state.
(9) Melanosomes would be captured when they came into contact with the region of the MT plus end decorated with CLIP-170, based on our experimental measurement of the length of this segment, and this would occur with a probability of success of 75%, also based on our experimental data.

Stochastic model details. In the model, radial MTs displayed dynamic instability at their free plus ends, which was modeled as growth of plus ends towards the cell periphery with the velocity υ_{m_+}, (MT growth, state M_+), shrinkage towards the center with velocity υ_{m_-} (MT shortening, state M_-), or pause (no net growth or shrinkage) (Suppl. Fig. 1A, growth, shortening and pause states M_+,

M_{-}, and M_0, respectively,). The rates of transitions between these states were denoted by the transition rate constants q_1 - q_6 (Suppl. Fig. 1B).

Melanosomes were modeled as point objects with the radius R_g=0.25 μm based on experimental measurements. Those melanosomes that were not bound to MTs (state *G* in Suppl. Figs. 1A and 1B) underwent actin-dependent random movement approximated by diffusion with the effective diffusion coefficient of 3 x 10^{-3} μm^2/sec measured in our previous study (Semenova et al., 2008). When the distance between the melanosome center and growing plus end of a MT became less than or equal to R_g, the melanosome bound to the MT tip and initiated MT-based movement. Initiation of movement occurred only if the melanosome bound to the MT at a distance from the tip that did not exceed the average length MT segment decorated with CLIP-170. On average, 74.9 ± 15.7% (mean ± SD) of binding events led to initiation of movement (Lomakin et al., 2009). MT-based movement involved stochastic transitions of melanosomes between three states: uninterrupted displacement towards the MT plus end with an average velocity υ_{g+}, towards the minus-end with velocity υ_{g-}, or lack of movement (pause) (states G_{+}, G_{-}, and G_0, respectively, in Suppl. Fig. 1B). The rates of transitions between these states were characterized by the rate constants k_1 - k_6 (Suppl. Fig. 1B). All parameter values used in the model were inferred from the experimental data (Suppl. Table 1). The rate constants q_1 - q_6 and k_1 - k_6 were calculated from the parameters of MT dynamic instability and statistics of pigment granule movement as described in (Slepchenko et al., 2007).

Methods. The model was solved stochastically using kinetic Monte Carlo simulations (Kraikivski et al., 2008 and 2010). In the simulations, the system was advanced in time with a time $\Delta t \approx 1/\sum R$, where $\sum R$ is a sum of all possible transition rates in the system. The probability of a change in the state of a melanosome or a MT tip over Δt equals the product of corresponding transition rates and Δt. Initially, MT tips were randomly distributed along the cell radius, and melanosomes were homogeneously dispersed within the cell area. Pigment density kinetics was computed for parameters of MT dynamic instability measured for cells stimulated to aggregate and disperse melanosomes (Table 1 of main text) and melanosome movement statistics were determined for melanophores treated with melanosome aggregation stimuli (Suppl. Table 1). Based on our previous work, we know that these simulations faithfully reproduce the kinetics of pigment granule aggregation that was measured experimentally under two conditions: an aggregation stimulus and treatment with the microtubule stabilizing drug Paclitaxel (Taxol) (Lomakin et al., 2009).

Effect of boundary. We rigorously tested the stochastic model to determine how major assumptions about the behavior of MTs at the cell boundary would affect the results of melanosome distribution in the simulations. We compared the kinetics of melanosome aggregation if growing MT plus ends immediately began shortening when they reached the cell margin or if they stopped growing and either paused or shortened based on the experimentally observed transition frequencies of these events as illustrated in Fig 1B. The results of simulations are shown in Suppl. Fig. 2. Change in the boundary conditions affected only MT tip density in the vicinity of the cell margin (Suppl. Fig. 2A). Importantly, both boundary behaviors gave essentially the same results for the the kinetics of melanosome aggregation (Suppl. Fig. 2B). Therefore, the stochastic model is robust and changes in boundary conditions do not significantly affect the outcome of simulations.

Continuous coarse-grained analysis.

Based on our finding that CLIP-170 is required for MT capture and is only located on MT tips, we predicted that only MT tips could capture granules. However, it is also possible that granules could become attached along the length of the MT. We evaluated the assumption that only MT tips could capture granules by determining that this capture by microtubule tips is completely sufficient to account for the kinetics of granule aggregation. In this approach, we described the system of granules and microtubule tips in terms of their densities rather than treating them as individual entities and treated their interactions as equilibrium kinetics. The aggregation dynamics was characterized by two processes: binding of pigment granules to growing MT tips and transport of the bound granules by molecular motors towards the center of the cell.

Binding. To describe the binding of granules to MTs, we distinguished two granule states: i) granules that performed the bidirectional motion along MTs are referred to MT-bound granules and ii) granules that were not bound to MTs were referred to as unbound. Two variables $G_b(r,t)$, $G_{ub}(r,t)$ were introduced to describe densities of granules in the MT-bound and MT-unbound states. All variables were assigned in the polar coordinate system because to a good approximation the angular distributions of granules and MT plus tips were uniform and their density variations occurred only along radial coordinate r (distance from the cell center along the cell radius). MT-unbound granules could be captured by MT plus ends and become MT-bound granules. This transition was defined by the binding rate $k_b G_{ub} \rho_m$, where ρ_m was the density of MT plus ends and k_b is the binding rate constant that characterized the rate with which MT plus ends captured the MT-unbound granules. The binding rate constant k_b was estimated as it is usually done in the kinetic theory for molecular gas. For two-dimensional case, the collision area for growing MT tips and granules was $(2R_g + \delta)\upsilon t$, where $\upsilon \cdot t$ is the average distance traveled by MT tips in time t with velocity υ, and the sum of granule and MT cross-sections $(2R_g + \delta)$ represents the distance at which MT plus tips are in contact with granules. The number of unbound granules in the collision area expected to be captured by a growing MT tip equals to $G_{ub}(2R_g + \delta)\upsilon t$, and the collision frequency for N_{m+} growing MT tips is $N_{m+} G_{ub}(2R_g + \delta)\upsilon$. Therefore, the binding rate constant can be estimated from the expression: $k_b = (2R_g + \delta)\upsilon$.

Transport. To describe the movement of granules to the cell center, we assumed that granules bound to MTs were moved by molecular motors with velocity $\upsilon_g = (P_{g-}\upsilon_{g-} - P_{g+}\upsilon_{g+})$, where $\upsilon_{g+}, \upsilon_{g-}$ are velocities of granule plus-end and minus-end runs, and P_{g+}, P_{g-} are probabilities of each direction of movement (Suppl. Table 1). The bulk transport of bound granules towards the cell center that resulted in the change of granule density was modeled as advection (directional movement of granules) $\upsilon_g \frac{1}{r}\frac{\partial r G_b(r,t)}{\partial r}$ written in a polar coordinate system.

Overall, the dynamics of bound and unbound granules, which took into account binding of granules to growing MT tips and their movement to the cell center, was described by the following system of equations:

$$\frac{\partial G_b(r,t)}{\partial t} = k_b G_{ub} \rho_m - \upsilon_g \frac{1}{r} \frac{\partial r G_b(r,t)}{\partial r} \qquad (1)$$

$$\frac{\partial G_{ub}}{\partial t} = -k_b G_{ub} \rho_m .$$

In the first equation that corresponded to the dynamics of bound (moving) granules the first term $k_b G_{ub} \rho_m$ describes the binding of granules to MT tips, and the second term $\upsilon_g \frac{1}{r} \frac{\partial r G_b(r,t)}{\partial r}$ describes the movement of these bound granules to the center of the cell. In the second equation of this system that corresponded to the dynamics of unbound granules the term - $k_b G_{ub} \rho_m$ represents decrease of unbound granule population. Diffusion of pigment granules not bound to MTs was slow and thus neglected in the Eqs. (1).

Equations 1 were solved in the circular cell geometry (radial coordinate *r* changes between zero and 27 (the cell radius *R* as shown in the Suppl. Fig. 3A) with the following initial conditions for granule densities: $G_{ub}\,|_{t=0} = G_{ub0} \cdot \eta(R-r)$ and $G_b\,|_{t=0} = 0$, where G_{ub0} is initial density of uniformly distributed unbound granules. The unit step function $\eta(R-r)$ equals 0 if *r*>R and 1 if *r*≤R, which indicates that initial distribution of pigment granules is confined to the area delineated by the cell outline. According to experimental data, the density of MT plus ends in cells with aggregated melanosomes is approximately uniform ($\rho_m \approx 0.1\ \mu m^{-2}$, Fig. 3B of the main text). For this case, equations 1 could be solved analytically (to give an exact solution). We obtained the following time-dependence of melanosome distributions along the cell radius:

$$G_{ub} = G_{ub0} e^{-k_b \rho_m t}, \text{ for } R_0 < r < R$$

$$G_b(r,t) = \frac{G_{ub0}}{k_b \rho_m r}\left(\upsilon_g e^{-k_b \rho_m t}(1-\eta(r-R)) + (k_b \rho_m \tilde{r} - \upsilon_g)(1-\eta(\tilde{r}-R)) + (k_b \rho_m R - \upsilon_g)(\eta(\tilde{r}-R) - \eta(r-R))\right), \qquad (2)$$

where the first equation corresponds to unbound granules, and the second equation MT-bound granules. In the second equation $\tilde{r} = r + \upsilon_g t$. The solutions for the total melanosome density that includes both bound and unbound granules G_b+G_{ub} in the region [R_0, R] at three different times are shown in Suppl. Fig. 4.

We used two approaches to determine the vaule for k_b in Equation 2, curve fitting to our experimental observations and using equilibrium kinetics. In the first approach, we systematically changed the value for k_b (Eq 2) to fit pigment granule aggregation kinetic curves measured in experiment. To generate the experimental curve, we obtained time-sequences of bright-field images of melanophores stimulated to aggregate pigment granules and measured the integrated pixel value $I(t)$ within a cell outline for each of the acquired images, as described in detail in Lomakin et al., 2009. The grey level was expressed as a percentage of the total initial level and was calculated for each image using the equation $(I_b - I(t))/(I_b - I(0)) \times 100$ where I_b was the averaged background pixel intensity value measured outside cell outlines, $I(t)$ was integrated pixel value within the cell outline at a given moment *t,* and $I(0)$ was the integrated

pixel value within a cell outline in the fully dispersed state (assigned to be 100%). For fitting of experimental curve we computed the kinetics of grey levels using the following equation:

$$\text{Percentage of grey levels} \approx \frac{2\pi \int_{R_0}^{R} (G_b + G_{ub}) r dr + G_{ub0} \pi R_0^{\,2}}{G_{ub0} \pi R^2} 100\% \quad (3)$$

that defines the fraction of area occupied by pigment granules. In this equation, $2\pi \int_{R_0}^{R} (G_b + G_{ub}) r dr$ describes the number of pigment granules located between the cell margin and the margin of the pigment granule mass in the cell center in the fully aggregated state (between R_0 and R in Suppl. Fig. 2A), and $G_{ub0} \pi R_0^{\,2}$ represents the number of pigment granules in the area occupied by the central pigment granule mass (grey area in Suppl. Fig. 3A). The value for the fully dispersed state $G_{ub0} \pi R^{\,2}$ was taken as 100%. The best fit of the experimental data with computational results (Suppl. Fig. 5) produced the value for k_b of 0.027 μm^2/s.

In the second approach, we estimated the value for k_b by computing the collision frequency between pigment granules and growing MT tips using equilibrium kinetics. As indicated above (page 3 of Supplemental Text, the collision rate depends on the net velocity of MT growth $\upsilon = (P_{m+}\upsilon_{m+} - P_{m-}\upsilon_{m-})$ and the sum of granule and MT diameters $(2R_g + \delta)$. The binding rate equals $k_b G_{ub} \rho_m = \upsilon(2R_g + \delta) G_{ub} \rho_m$ and thus the collision rate constant k_b can be computed using experimental data (probabilities of MT growth (M_+) and shortening (M_-) states, velocities of MT growth and shortening, melanosome radius, and MT diameter (Suppl. Table 1)). The value for k_b computed using the equation $k_b = (P_{m+}\upsilon_{m+} - P_{m-}\upsilon_{m-})(2R_g + \delta)$ is 0.02 μm^2/s. This value is close to the k_b value of 0.027 μm^2/s estimated by the other method. We conclude that the results of our analysis are consistent with the assumption that granules are captured only by growing MT tips.

Supplemental References.

Kraikivski, P., B. M. Slepchenko, and I.L. Novak. (2008). Actin bundling: initiation mechanisms and kinetics. Phys. Rev. Lett. *101*, 128102-1-128102-4.

Kraikivski P., and B. M. Slepchenko. 2010. Quantifying a pathway: Kinetic analysis of actin dendritic nucleation. *Biophys. J.* 99(3) 708-715

Lomakin, A.J., Semenova, I., Zaliapin, I., Kraikivski, P., Nadezhdina, E., Slepchenko, B.M., Akhmanova, A., and Rodionov, V. (2009). CLIP-170-dependent capture of membrane organelles by microtubules initiates minus-end directed transport. Dev Cell *17*, 323-333.

Semenova, I., A.Burakov, N.Berardone, I.Zaliapin, B.M.Slepchenko, T.Svitkina, A.Kashina, and V.Rodionov. (2008). Actin dynamics is essential for myosin-based transport of membrane organelles. Curr. Biol. *18*, 1581-1586.

Slepchenko, B.M., I. Semenova, I. Zaliapin, and V. Rodionov. (2007). Switching of membrane organelles between cytoskeletal transport systems is determined by regulation of the microtubule-based transport. J. Cell Biol. *179*, 635–641

Supplemental Figures.

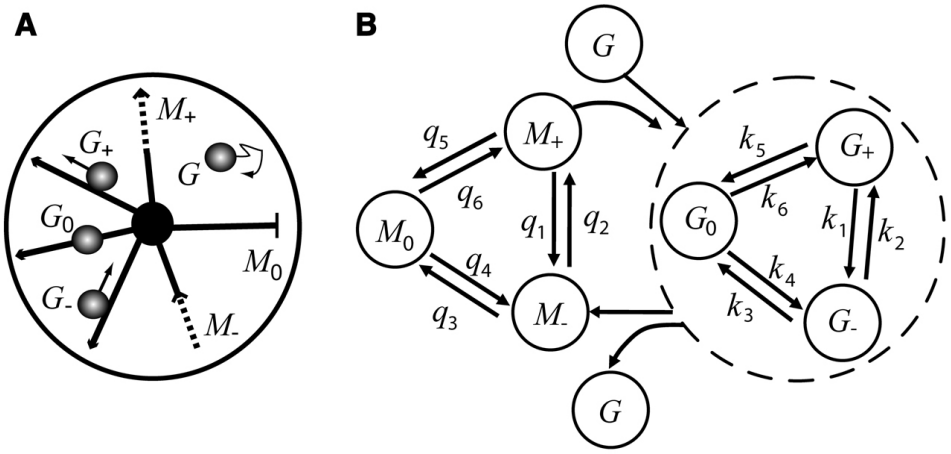

Supplemental Figure 1. Computational model for melanosom e aggregation. (A) Schematic representation of melanosome movements and MT dynamics included in computational model. At any given moment of time, each MT can be in one of three dynamic states: growth (M_+), shortening (M_-), or pausing (M_0). A melanosome either undergoes actin-dependent random walk (state G), or is bound to MT. The MT-bound states of a melanosome include plus-end runs (G_+), minus-end runs (G_-), and pauses (G_0). (B) Schematic representation of switching events; wiring diagram for MT states with corresponding rate constants q_1 - q_6 (left) is coupled to melanosome transitions with rate constants k_1 - k_6 (right) through the collision-controlled binding of the melanosome to a growing MT tip. Reproduced from Lomakin et al., 2009, with permission from Elsevier.

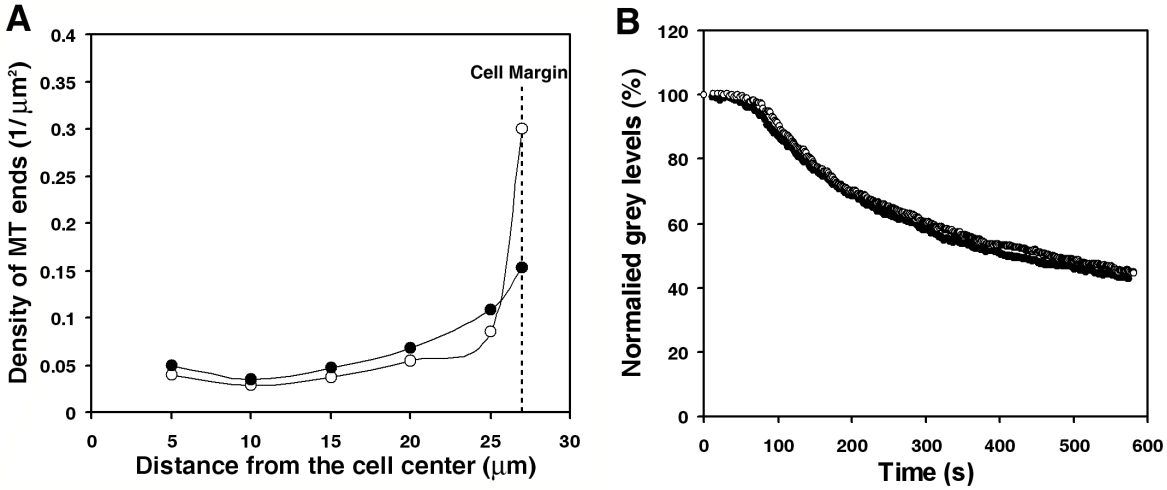

Supplemental Figure 2. Computed distribution of growing MT plus ends and kinetics of melanosome aggregation for different boundary conditions at the cell margin. (A). Distribution of growing MT plus ends and (B) kinetics of pigment aggregation computed using the assumption that growing MTs begin immediate shortening when they reach the cell margin (closed circles) or pause and start shortening with a probability determined by the transition frequencies determined experimentally (Fig 1).

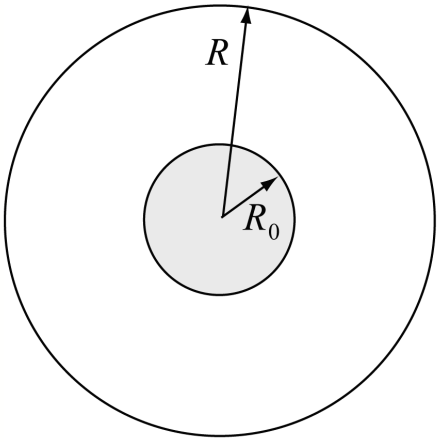

Supplemental Figure 3. Geometries of cell and aggregate of pigment granules used to solve Equations1. R, cell radius; R_0, radius of pigment granule mass in the fully aggregated state.

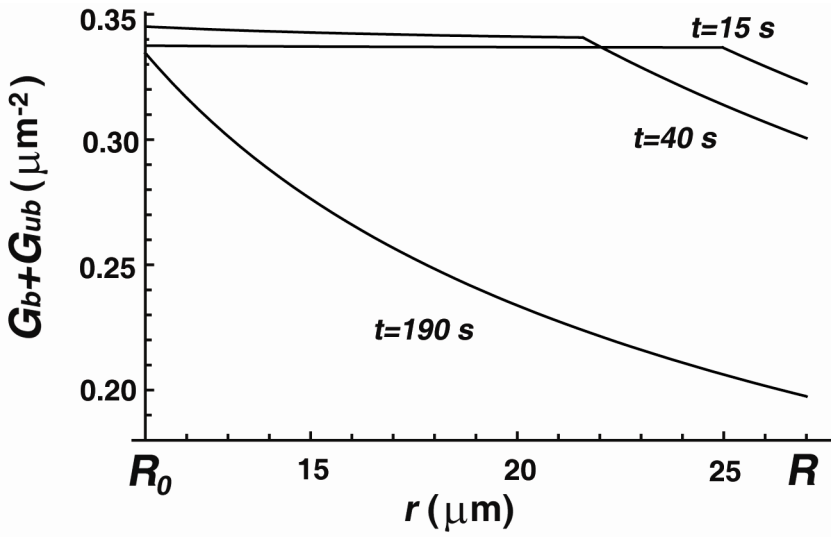

Supplemental Figure 4. The solutions for the total pigment granule density that includes both bound and unbound granules at three different time intervals after initiation of melanosome aggregation. The results are shown for t =15, 40, and 190 s after stimulation of pigment granule aggregation. The values for the other parameters used in the simulations were: R_0=11 μm, R=27 μm, υ_g =0.135 μm/s, G_{ub0}=0.34 μm^{-2}, $\rho_m \approx$0.1 μm^{-2}, k_b = 0.027 μm^2/s.

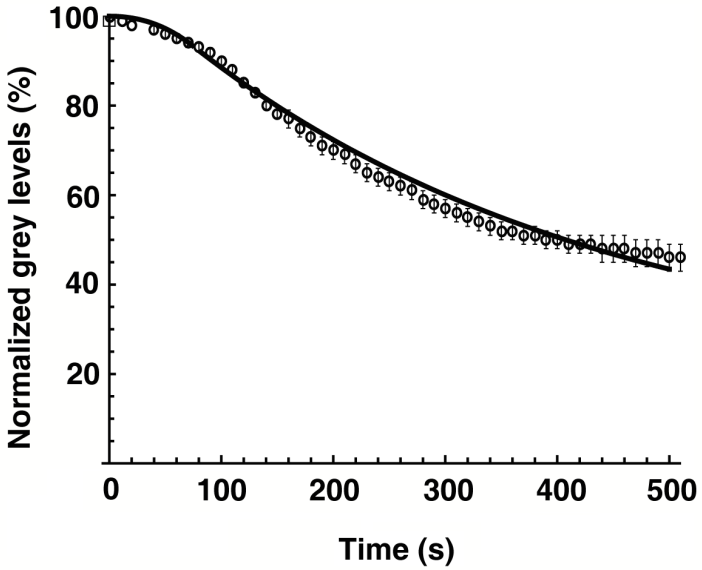

Supplemental Figure 5. Best fit of the experimental data to the computational data used to determine k_b. Experimental data (open circles) were fitted with the solution of Equations (1), by changing the value of the fitting parameter k_b (solid line); values for other parameters used in simulations were: R_0=11 μm, R=27 μm, υ_g =0.135 μm/s, G_{ub0}=0.34 μm^{-2}, $\rho_m \approx$0.1 μm^{-2}. Best fit was obtained at k_b = 0.027 μm^2/s.

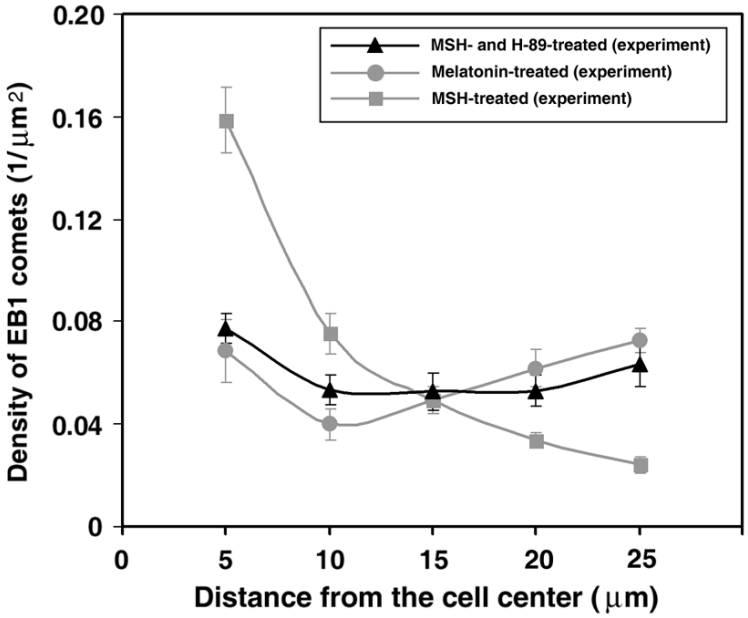

Supplemental Figure 6. Experimentally measured distribution of growing MT plus ends along the cell radius in melanophores treated with the PKA inhibitor H89. The density of growing MT plus ends was determined experimentally by immunostaining melanophores with antibodies against EB1 as shown in Fig. 2A. In H89-treated cells, the distribution of growing MT plus ends (black triangles) along the cell radius was similar to cells with aggregated pigment granules (grey circles) and differed from melanophores with dispersed melanosomes (grey squares).

Supplemental Table 1. Parameters used in the computational model for pigment aggregation.

	Notation	Values	
		Melatonin (aggregated pigment)	**MSH (dispersed pigment)**
Cell radius (μm)	R	27	
Diffusion of unbound melanosome ($\mu m^2/s$)	D	$3x10^{-3}$	
Melanosome radius (μm)	R_g	0.25	
MT cross-section (μm)	δ	0.025	
Comet tail length (μm)		1.2	
Total number of melanosomes	N_g	770	
Total number of MTs	N_m	370	160
Rate constant for $M_- \rightarrow M_+$ (s^{-1})	q_2	0.068	0.0389
Rate constant for $M_- \rightarrow M_0$ (s^{-1})	q_3	0.016	0.0018
Rate constant for $M_+ \rightarrow M_0$ (s^{-1})	q_5	0.02	0.0071
Rate constant for $M_0 \rightarrow M_-$ (s^{-1})	q_4	0.070	0.0472
Rate constant for $M_0 \rightarrow M_+$ (s^{-1})	q_6	0.156	0.2426
Rate constant for $M_+ \rightarrow M_-$ (s^{-1})	q_1	0.04	0.0295
Probability of MT state M_+	P_{m+}	0.6037	0.5595
Probability of MT state M_-	P_{m-}	0.3222	0.4242
Velocity of MT growth (μm/s)	υ_{m_+}	0.16	0.23
Velocity of MT shortening (μm/s)	υ_{m_-}	0.18	0.25
Rate constants for $G_- \rightarrow G_+$ (s^{-1})	k_2	0.587	
Rate constants for $G_- \rightarrow G_0$ (s^{-1})	k_3	0.374	
Rate constants for $G_+ \rightarrow G_0$ (s^{-1})	k_5	0.274	
Rate constants for $G_0 \rightarrow G_-$ (s^{-1})	k_4	0.8	
Rate constants for $G_0 \rightarrow G_+$ (s^{-1})	k_6	0.176	
Rate constants for $G_+ \rightarrow G_-$ (s^{-1})	k_1	1.948	
Probability of granule state G_+	P_{g+}	0.1702	
Probability of granule state G_-	P_{g-}	0.5643	
Velocity of melanosome minus-end runs (μm/s)	υ_{g_-}	0.344	
Velocity of melanosome plus-end runs (μm/s)	υ_{g_+}	0.345	
Simulation time step (s)	Δt	10^{-3}	